

Ultra high energy cosmic rays from super-heavy dark matter in the context of large exposure observatories

A. D. Supanitsky^{a,1} and G. Medina-Tanco^b

^aInstituto de Tecnologías en Detección y Astropartículas (CNEA, CONICET, UNSAM),
Centro Atómico Constituyentes, San Martín, Buenos Aires, Argentina.

^bInstituto de Ciencias Nucleares, UNAM,
Circuito Exterior S/N, Ciudad Universitaria, México D. F. 04510, México.

E-mail: daniel.supanitsky@iteda.cnea.gov.ar, gmtanco@nucleares.unam.mx

Abstract. The origin of the ultra high energy cosmic rays (UHECRs, $E > 10^{18}$ eV) is still uncertain. However, great progress has been achieved due to the data taken by The Pierre Auger and Telescope Array observatories. The UHECR flux presents two main features, a hardening of the spectrum known as the ankle and a suppression at higher energies. The experimental data suggest that above the ankle the UHECRs flux is dominated by an extragalactic component of astrophysical origin. However, a minority component of exotic origin that dominates the flux beyond the suppression is still compatible with current data. Therefore, there exist the possibility that part of the UHECR flux originates from the decay of super-heavy dark matter particles clustered in the halos of the galaxies. In these scenarios the main contribution comes from the halo of our galaxy. In this article the possibility of identifying these scenarios in the context of the future very large exposure cosmic rays observatories is studied. It is worth mentioning that the contribution of the extragalactic halos located in the nearby universe is also included in these studies.

¹Corresponding author.

Contents

1	Introduction	1
2	Cosmic rays from galactic and extragalactic SHDM	2
3	Conclusions	11
A	Cosmic rays of astrophysical origin	12
B	Angular distribution	12
C	Required exposure for larger minimum energy	13

1 Introduction

The nature of the ultra high energy cosmic rays (UHECRs, $E \geq 10^{18}$ eV) is still unknown. The main observables used to study its origin are the energy spectrum, the composition profile as a function of primary energy, and the distribution of their arrival directions.

The UHECR flux has been measured with good statistics by the Pierre Auger Observatory and Telescope Array. It presents two main features, a hardening at $\sim 10^{18.7}$ eV, known as the ankle and a suppression. This suppression is observed by Auger at $10^{(19.62 \pm 0.02)}$ eV and by Telescope Array at a larger energy, $10^{(19.78 \pm 0.06)}$ eV [1]. Also, the Auger spectrum takes smaller values than the ones corresponding to Telescope Array. The discrepancies between the two observations can be diminished by shifting the energy scales of both experiments within their systematic uncertainties. However, some differences are still present in the suppression region [1].

The composition of the UHECRs is determined by comparing experimental data with air shower simulations, which makes use of high energy hadronic interaction models. These models present non negligible systematic uncertainties since the hadronic interactions at the highest energies cannot be deduced from first principles. As a consequence, the composition determination is subject to important systematic uncertainties. One of the most sensitive parameters to the nature of the primary is the atmospheric depth of the maximum shower development, X_{max} . It can be obtained on an event by event basis from the data taken by the fluorescence telescopes of Auger and Telescope Array. The mean value of X_{max} obtained by Auger [2], interpreted by using the updated versions of current high energy hadronic interaction models, shows that the composition is light from $\sim 10^{18}$ up to $\sim 10^{18.6}$ eV. From $\sim 10^{18.6}$ eV, the composition becomes progressively heavier for increasing values of the primary energy. This trend is consistent with the results obtained by using the standard deviation of the X_{max} distribution [2]. On the other hand, the X_{max} parameter reconstructed from the data taken by the fluorescence telescopes of Telescope Array is also compatible with a light composition at energies below the ankle, when it is interpreted by using the current hadronic interaction models [3]. It is worth mentioning that the X_{max} distributions, as a function of primary energy, obtained by Auger and Telescope Array are compatible within systematic uncertainties [4]. However, the presence of heavier primaries at energies above the ankle cannot be confirmed by the Telescope Array data due to the limited statistics of the event sample [4].

The distribution of the arrival directions of the events with primary energies above $\sim 10^{18.9}$ eV detected by Auger presents an anisotropy that can be described as a dipole of $\sim 6.5\%$ amplitude [5]. The significance of this detection is larger than 5.2σ . The dipole direction is such that a scenario in which the flux is dominated by a galactic component is disfavored [5]. Regarding point source searches, Auger has found an indication of a correlation between the arrival directions of the events of primary energy larger than $10^{19.6}$ eV and nearby starburst galaxies [6]. The significance of this correlation is at $\sim 4\sigma$ level. Also the Auger data present an excess above $10^{19.76}$ eV in the region of the radio galaxy Centaurus A [7, 8]. However, the statistical significance of this excess is $\sim 3.1\sigma$. The Telescope Array Collaboration has also found an excess above $10^{19.75}$ eV in a direction of the sky which is contained in the supergalactic plane [9, 10]. The statistical significance of this excess is $\sim 3.4\sigma$.

The experimental data suggest that the cosmic ray flux above the ankle is dominated by a component originated in extragalactic sources, most of those are possibly starburst galaxies. Besides, these sources accelerate not only protons but also heavier nuclei, assuming that current high energy hadronic interaction models do not present too large systematic uncertainties. However, a minority component of another origin that could dominate the flux beyond the suppression is still compatible with the experimental data [11].

The possibility that the by-products of the decay of unstable super-heavy dark matter (SHDM) particles can contribute to the UHECR flux has been studied extensively in the past (see for instance [12–17]). In these models the dark matter is composed of supermassive particles produced gravitationally during inflation [18–21]. These particles would be clustered in the halo of the galaxies including ours. The spectrum of SHDM particles is expected to be dominated by gamma rays, protons and neutrinos. The upper limits to the gamma-ray flux obtained by Auger and the non detection of events above $10^{20.3}$ eV by Auger impose tight constraints to the flux corresponding to this hypothetical SHDM component. Therefore, to test the hypothesis of the existence of this component, observatories of very large exposure are required. In this article we study the possibility to identify this scenario in the context of the next generation UHECR observatories which will have a much larger exposure than current ones. In this study, besides considering the contribution of the galactic halo, the contribution of extragalactic halos located in the nearby universe is also included.

2 Cosmic rays from galactic and extragalactic SHDM

The rest mass and the decay time of the SHDM particles are free parameters in models in which a minority component of the UHECRs originate from the decay of these unstable particles. In the energy range of interest these parameters are constrained by cosmic ray observations. In particular, the most restrictive constraints are imposed by the upper limits to the photon flux found by Auger [22] and also the non-observation by Auger of events above $10^{20.3}$ eV [11]. This last analysis imposes more restrictive constraints than the ones based on the upper limits to the photon flux for scenarios in which $M_X > 10^{23}$ eV. Therefore, the mass of the SHDM particles considered in this work is $M_X = 10^{22.3}$ eV, for which only the constraints coming from the upper limits to the photon flux obtained by Auger are relevant.

Given the mass of the SHDM particles the decay time corresponding to the scenario for the largest SHDM cosmic ray flux, compatible with the upper limits to the photon fraction obtained by Auger, can be estimated from the predicted integral gamma-ray flux, which is

given by,

$$J_\gamma(> E) = \frac{1}{4\pi M_X c^2 \tau_X} \sum_{s=1}^N \int_E^\infty dE' \frac{dN_{\gamma,s}}{dE'}(E', D_s) \int_0^\infty d\xi \int_0^{2\pi} d\alpha \int_0^\pi d\delta \cos \delta \times \rho_{X,s}(r(\xi, \alpha, \delta, \alpha_s, \delta_s)) \varepsilon(\delta), \quad (2.1)$$

where M_X is the rest mass of the SHDM particle, τ_X is its decay time, c is the speed of light, N is the number of dark matter halos considered, $\rho_{X,s}$ is the energy density of the s -th dark matter halo, r is the distance measured from the center of the halo to a given point in the space, α_s is the right ascension of the center of the s -th halo, δ_s is the declination of the center of the s -th halo, ξ is the distance from the Earth in the direction defined by the angles α and δ , $dN_{\gamma,s}/dE$ is the number of gamma rays per units of energy corresponding to a single decay including the effects of propagation, and D_s is the comoving distance from the Earth to the center of the s -th halo. Here $\varepsilon(\delta)$ is the relative exposure of Auger which fulfills the normalization condition,

$$\int_0^\pi d\delta \cos \delta \varepsilon(\delta) = 1. \quad (2.2)$$

An analytical expression for $\varepsilon(\delta)$ can be found in Ref. [23].

Gamma rays generated in SHDM decays can interact with low energy photons of the radiation field present in the universe during propagation. The relevant low energy photon backgrounds are the cosmic microwave background (CMB) and the radio background (RB). The main processes undergone by gamma rays are pair production ($\gamma + \gamma_b \rightarrow e^+ + e^-$) and double pair production ($\gamma + \gamma_b \rightarrow e^+ + e^- + e^+ + e^-$).

Gamma rays that originate in our Galaxy are assumed to propagate freely due to the fact that the distances traveled by them, from generation to the Earth, are much smaller than their mean free path. However, the spectrum of gamma rays, which originated from SHDM decays in extragalactic halos are modified due to the interactions undergone by them during propagation. Therefore, the energy spectrum of the gamma rays at Earth takes the following form,

$$\frac{dN_\gamma}{dE}(E, D) = \frac{dN_\gamma^0}{dE}(E) \quad \text{Galactic gamma rays} \quad (2.3)$$

$$\frac{dN_\gamma}{dE}(E, D) = \exp \left[-\frac{D}{\lambda_{\gamma\gamma}(E)} \right] \frac{dN_\gamma^0}{dE}(E) \quad \text{Extragalactic gamma rays}, \quad (2.4)$$

where dN_γ^0/dE is the energy distribution at decay, $\lambda_{\gamma\gamma}$ is the mean free path of gamma rays in the photon background, and D is the distance from the center of the halo to the Earth. Note that Eq. (2.4) is valid for a non-expanding universe which in our case is a good approximation, since the extragalactic halos considered are at distances smaller than ~ 140 Mpc.

The energy distributions $dN_{\gamma,p}/dE$ of the gamma rays and protons (the secondary particles considered in this work) generated from the decay of the SHDM particles are calculated by using the SHdecay program [24].

Figure 1 shows the mean free path of gamma rays in the CMB and RB for the relevant processes. The radio background model used for the calculation is the one developed in Ref. [25]. The calculation is performed by using the tools developed for the package CRPropa 3, which are accessible at Ref. [26]. It can be seen that for energies above 10^{19} eV the total

mean free path is larger than 1 Mpc, this is the reason that supports the assumption that gamma rays originated in the halo of our Galaxy propagate freely. It can also be seen that below $\sim 10^{19.5}$ eV the mean free path is dominated by pair production in the CMB, from $\sim 10^{19.5}$ eV to $\sim 10^{23.5}$ eV the relevant process is also pair production but in the RB, and finally above $\sim 10^{23.5}$ eV the dominant process is the double pair production in the CMB.

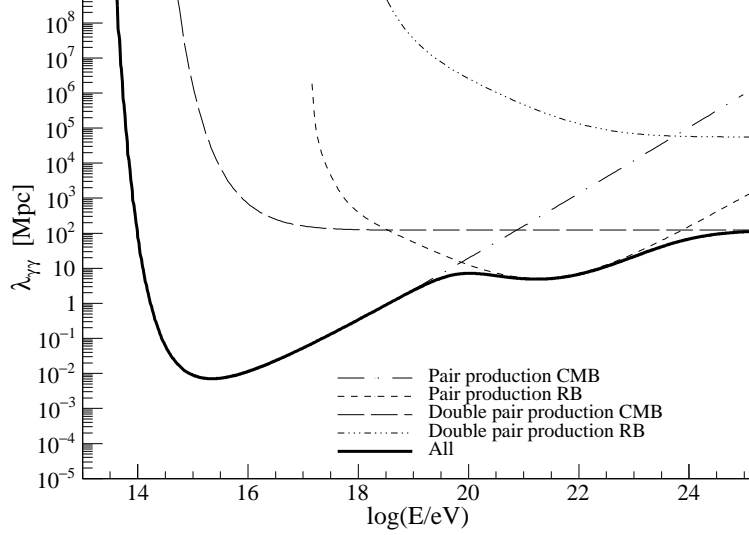


Figure 1. Mean free path of gamma rays in the CMB and RB as a function of the gamma ray energy.

The Burkert dark matter profile [27] is considered in this work. It is given by,

$$\rho_X(r) = \frac{\rho_B}{\left(1 + \frac{r}{r_B}\right) \left(1 + \left(\frac{r}{r_B}\right)^2\right)}, \quad (2.5)$$

where ρ_B and r_B depend on the halo under consideration. For the Milky Way the parameters are $\rho_B = 1.187 \text{ GeV cm}^{-3}$ and $r_B = 10 \text{ kpc}$ [28]. The dark matter halos considered are the ones of the DMCat catalog [29, 30], which is based on the galaxy group catalogs of Refs. [31, 32]. In that catalog there are 17021 halos with comoving distances smaller than $\sim 140 \text{ Mpc}$. The parameters of the Burkert profile corresponding to these extragalactic halos are can obtained from the catalog.

Figure 2 shows the integral gamma-ray flux obtained by using Eq. (2.1) for $\tau_X = 5.4 \times 10^{22} \text{ yr}$. This value for the decay time corresponds to the largest integral gamma-ray flux compatible with the Auger upper limits [33], which are also shown in the figure. The contributions of our galaxy and the one corresponding to the halos in the DMCat catalog are included.

The cosmic ray flux originated in SHDM decays for an observatory with uniform exposure is given by,

$$J_i(E) = \frac{1}{(4\pi)^2 M_X c^2 \tau_X} \sum_{s=1}^N \frac{dN_{i,s}}{dE}(E, D_s) \int_0^\infty d\xi \int_0^{2\pi} d\alpha \int_0^\pi d\delta \cos \delta \times \rho_{X,s}(r(\xi, \alpha, \delta, \alpha_s, \delta_s)), \quad (2.6)$$

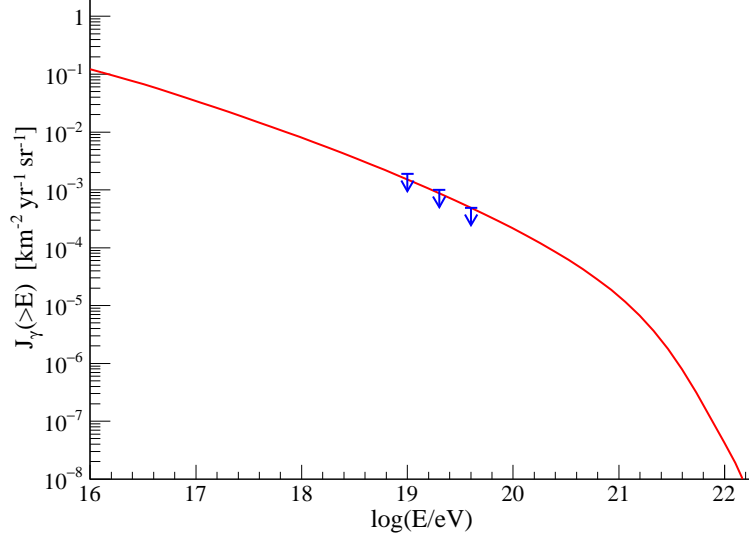


Figure 2. Integral gamma-ray flux as a function of the logarithm of the energy. The galactic and extragalactic (halos in the DMCat catalog) contributions are included. The arrows correspond to the 95% CL upper limits obtained by Auger [33].

where $i \in \{p, \gamma\}$, $dN_{\gamma, s}/dE$ is given by Eq. (2.3) for the galactic halo and Eq. (2.4) for the extragalactic halos, and

$$\frac{dN_p}{dE}(E, D) = \frac{dN_p^0}{dE}(E) \quad \text{Galactic protons} \quad (2.7)$$

$$\frac{dN_p}{dE}(E, D) = \int_0^\infty dE' P(E|E', D) \frac{dN_p^0}{dE'}(E') \quad \text{Extragalactic protons.} \quad (2.8)$$

Here dN_p^0/dE is the proton energy distribution at decay and $P(E|E', D)$ is the energy distribution of a proton at Earth with energy E injected at a comoving distance D with energy E' .

As well as gamma rays, extragalactic protons can undergo interactions with the low energy photon backgrounds during propagation through the Universe. The main processes are pair production ($p + \gamma_b \rightarrow p + e^+ + e^-$) and photopion production ($p + \gamma_b \rightarrow N + \pi s$, where N corresponds to nucleons). The distribution function $P(E|E', D)$ is obtained from simulations performed by using the CRPropa 3 package [34]. In this program all relevant processes are taken into account including also the interactions of the ultra high energy protons with the low energy photons of the extragalactic background light (see Ref. [34] for details).

Figure 3 shows the energy spectrum observed by Auger [35] fitted with the function defined in Ref. [35] (see appendix A). In the scenario considered in this work it is assumed that this component is of astrophysical origin. The Auger data are compatible with a SHDM component which starts to dominate the flux above 10^{20} eV. The SHDM contribution, which corresponds to the considered scenario in which $M_X = 10^{22.3}$ eV and $\tau_X = 5.4 \times 10^{22}$ yr is also shown in the figure. As before, the contributions of the galactic halo and the extragalactic halos from the DMCat catalog are included. From the figure it can be seen that the contribution from the extragalactic halos is a small fraction of the total SHDM flux. The propagation effects on the proton and gamma-ray components are also evident, in particular the proton component presents a pile-up originated from the photopion production process [36].

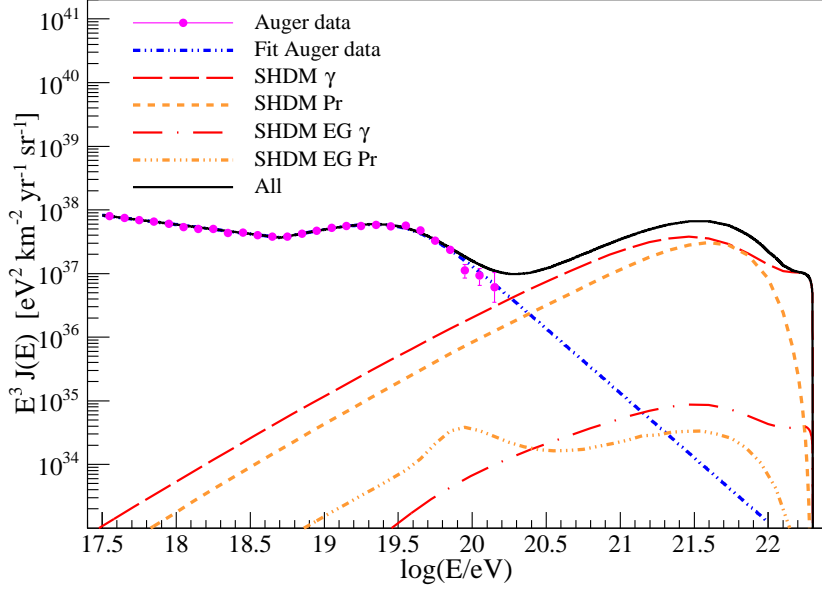


Figure 3. Ultra high energy cosmic ray flux as a function of the logarithm of the primary energy. The data points correspond to the Auger measurements [35]. Double dotted-dashed line corresponds to a fit of the Auger data. Dashed lines correspond to the proton and gamma-ray components originated from SHDM decays and the triple dotted-dashed and dotted-dashed lines correspond to the proton and gamma-ray contribution from the extragalactic halos of the DMCat catalog, respectively. Solid line corresponds to the total contribution.

One of the most important characteristic of next generation space-based UHECR observatories, like JEM-EUSO [37] and POEMMA [38], is its very large exposure. Fig. 4 shows the expected number of events originated from SHDM decays, corresponding to each halo in the DMCat catalog, as a function of the comoving distance for a constant exposure of $\mathcal{E} = 10^6$ km² yr sr above 10²⁰ eV [38]. The left panel of the figure shows the separated proton and gamma ray contributions and the right panel shows the sum of these two. Note that the number of events corresponding to proton (photon) primaries is given by the integral of the corresponding term in Eq. (2.6) above 10²⁰ eV, with $i = p$ ($i = \gamma$), multiplied by the exposure \mathcal{E} . From the left panel of the figure it can be seen that the number of events corresponding to gamma rays decreases much faster with the comoving distance than the one corresponding to protons. This is due to the fact that the gamma rays undergoing interactions are removed from the flux but protons, or more precisely nucleons, lose a fraction of their energy in each interaction but they still contribute to the flux. From the right panel of the figure it can be seen that there is only one halo, located close to the Earth, for which the expected number of events is of order one. For the rest of the halos is smaller than ~ 0.3 . The halo that most contributes to the number of events corresponds to the Andromeda galaxy, also known as M31. Note that in the two plots of Fig. 4 two different regions can be identified, which are separated at a comoving distance of ~ 55 Mpc. These two regions correspond to the two different galaxy catalogs used to build the DMCat catalog [29].

Although the contribution from a given extragalactic halo is much smaller than the one corresponding to the galactic halo, it can be important due to the fact that the gamma rays and protons originating in such halo come from a narrow region of the sky. Therefore, in that region the contribution of the extragalactic halo can be more important than the one

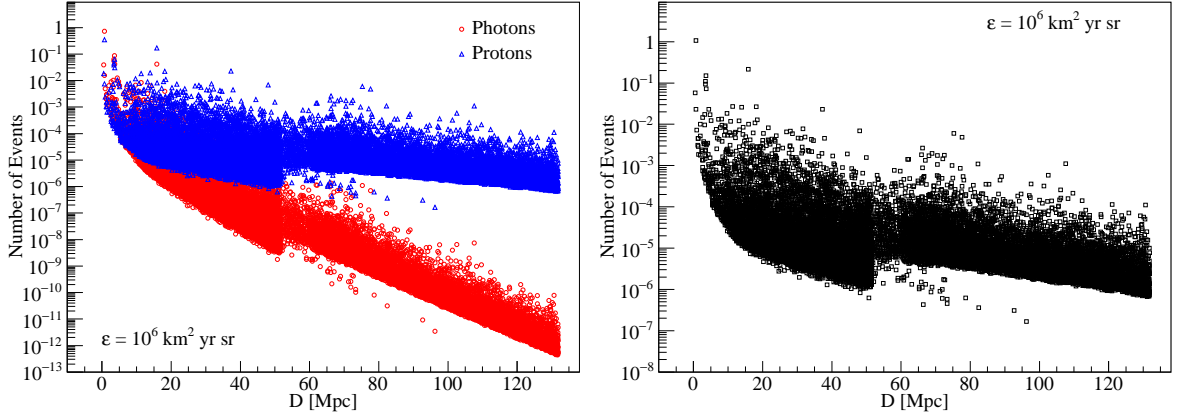


Figure 4. Expected number of events originated from SHDM decays, corresponding to each halo in the DMCat catalog, as a function of the comoving distance D for exposure $\mathcal{E} = 10^6 \text{ km}^2 \text{ yr sr}$ and energy above 10^{20} eV . Left panel: expected number of events for protons and gamma rays. Right panel: total number of events irrespective of the type.

corresponding to our galaxy, specially in regions far from the galactic center where the galactic contribution decreases considerably. In order to study this possibility the angular distribution of gamma rays and proton is required. The flux from a given halo, s , is given by,

$$J_{s,i}(E, \theta) = \frac{\text{sr}^{-1}}{4\pi M_X c^2 \tau_X} \frac{dN_{s,i}}{dE} \left[2 \Theta\left(\frac{\pi}{2} - \theta\right) \int_{D_s \sin \theta}^{D_s} dr \frac{r \rho_{X,s}(r)}{\sqrt{r^2 - D_s^2 \sin^2(\theta)}} + \int_{D_s}^{\infty} dr \frac{r \rho_{X,s}(r)}{\sqrt{r^2 - D_s^2 \sin^2(\theta)}} \right], \quad (2.9)$$

where $\Theta(x)$ is the Heaviside function (i.e. $\Theta(x) = 1$ for $x \geq 0$ and $\Theta(x) = 0$ otherwise) and $\theta \in [0, \pi]$ is the angle between the direction of the center of the halo and the direction of observation. Note that, for the Burkert dark matter profile, the integral in Eq. (2.9) can be done analytically (see appendix B for details).

Figure 5 shows the angular distribution calculated from Eq. (2.9) (see appendix B), normalized to its value at $\theta = 0$, for the Milky Way (left panel) and Andromeda (right panel). It can be seen from the figure that even though the distribution of Andromeda is much narrower than the one corresponding to the Milky Way, it has a non negligible angular width, which is larger than 4° .

The HEALPix library [39] is used to study the contribution of the different UHECRs sources in a given region of the sky. It is assumed that the arrival directions of the cosmic rays of astrophysical origin are uniformly distributed. Given a pixelization of the sphere the average number of events with primary energies above E_{min} and arrival directions contained in the j -th pixel is $\langle n_j \rangle(E_{min}) = \langle n_j \rangle_{Astro}(E_{min}) + \langle n_j \rangle_{SHDM}(E_{min})$, where

$$\langle n_j \rangle_{Astro}(E_{min}) = \mathcal{E} \frac{\Omega_j}{4\pi} \int_{E_{min}}^{\infty} dE J_{Astro}(E), \quad (2.10)$$

$$\langle n_j \rangle_{SHDM}(E_{min}) = \mathcal{E} \frac{1}{4\pi} \int_{E_{min}}^{\infty} dE \int_{\Omega_j} dl db \cos b \sum_{s=1}^N \sum_{i=\gamma, p} J_{s,i}(E, l, b). \quad (2.11)$$

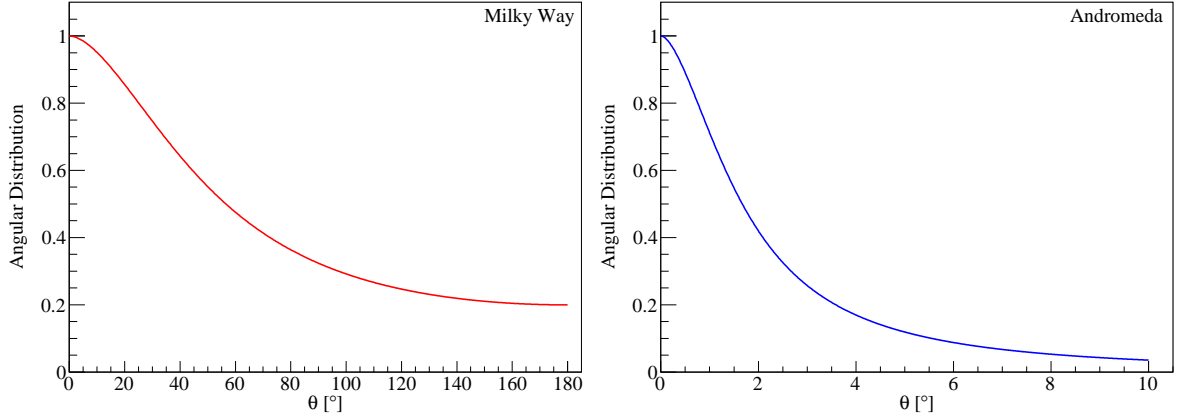


Figure 5. Angular distribution, normalized to its value at $\theta = 0$, as a function of θ for the Milky Way (left panel) and for Andromeda (right panel).

Here $\langle n_j \rangle_{Astro}(E_{min})$ corresponds to the average number of events of astrophysical origin, Ω_j is the solid angle subtended by the j -th pixel, $J_{Astro}(E)$ is the flux of astrophysical origin (see appendix A), $\langle n_j \rangle_{SHDM}(E_{min})$ corresponds to the average number of events for the SHDM component, l and b are the galactic longitude and the galactic latitude, respectively, and $J_{s,i}(E, l, b)$ is given by Eq. (2.9) but written as a function of the galactic coordinates. Note that an observatory with uniform exposure is considered.

A pixelization of the sphere with 768 pixels is considered (corresponding to $N_{side} = 8$ [39]). In this pixelization each pixel has an angular radius of the order of 4° . It is worth mentioning that the reconstruction uncertainties are not included in the calculation because at these energies the angular resolution is in general smaller than 1° [38], which is much smaller than the pixel radius. The angular integrals in Eq. (2.11) are performed by using the Monte Carlo technique. The left panel of Fig. 6 shows the average number of events expected in each pixel for the extragalactic halos from the DMCat catalog, $E_{min} = 10^{20}$ eV, and $\mathcal{E} = 10^6$ km² yr sr. Note that the scale color is logarithmic. From the figure it can be seen that the region in the sky for which the average number of events is larger corresponds to the surroundings of Andromeda. However, a larger exposure is required in order to increase the probability of observing at least one event in the pixels of the surroundings of Andromeda. The right panel of the figure shows the average total number of events, which includes the contributions from the decay of SHDM in the galactic halo, SHDM in the DMCat catalog halos, and the astrophysical component. It can be seen that the galactic halo dominates the average total number of events. However, Andromeda is placed in a region far from the galactic center, then its contribution can be significant, provided the total exposure is larger.

The probability to observe a given number of events in a given pixel follows the Poisson distribution. This probability strongly depends on the scenario considered. In particular, for a given value of the exposure, the probability to observe at least one event in the pixels corresponding to the galactic center region is larger for the case in which the contribution from the SHDM decays is non negligible. The probability to observe at least one event in the j -th pixel is given by,

$$P(n_j \geq 1 | E_{min}) = 1 - \exp(-\mu_j), \quad (2.12)$$

where $\mu_j = \langle n_j \rangle(E_{min})$ or $\mu_j = \langle n_j \rangle_{Astro}(E_{min})$ for the cases in which the SHDM contribution

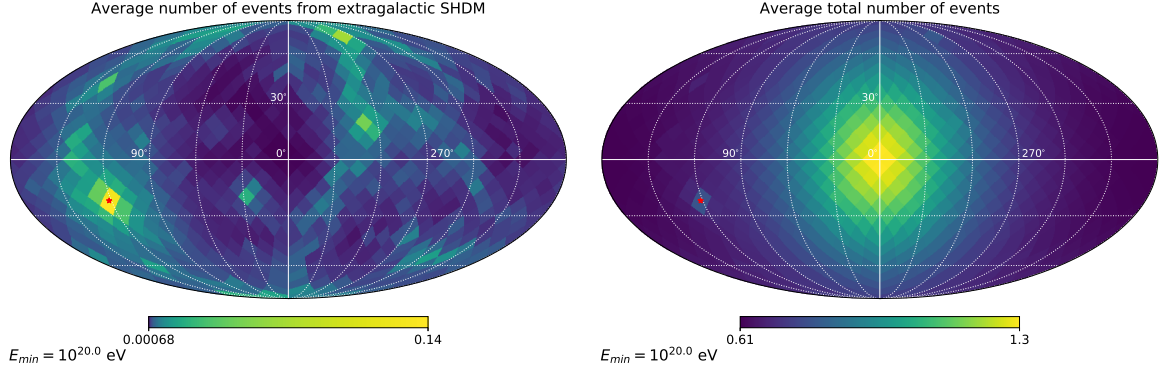


Figure 6. Left panel: Average number of events for the extragalactic halos from the DMCat catalog, a logarithmic scale color is considered in this case. Right panel: Average total number of events including the contributions from the decay of SHDM in the galactic halo, SHDM in the DMCat catalog halos, and the astrophysical component. Here $E_{min} = 10^{20}$ eV and $\mathcal{E} = 10^6$ km² yr sr. The red star corresponds to the position of Andromeda.

is non negligible and negligible, respectively. Therefore, the exposure required to measure at least one event in the j -th pixel with probability p_0 is given by,

$$\tilde{\mathcal{E}}_j(p_0) = -\frac{1}{\mu_j} \ln(1 - p_0). \quad (2.13)$$

The left panel of Fig. 7 shows the exposure required to observe at least one event in each pixel with 0.95 probability, i.e. $\tilde{\mathcal{E}}_j(0.95)$ for $E_{min} = 10^{20}$ eV and for the case in which the contribution from SHDM is non negligible. It can be seen that $\tilde{\mathcal{E}}_j(0.95)$ corresponding to the pixels in the center of the galaxy is more than two times smaller than the one corresponding to the regions far from the galactic center. In the case of the Andromeda region $\tilde{\mathcal{E}}_j(0.95)$ has to be ~ 1.3 times smaller compared to regions far from the galactic center. The right panel of Fig. 7 shows the ratio between $\tilde{\mathcal{E}}_j(0.95)$ for the scenario with a negligible SHDM contribution and for the one with a non negligible SHDM contribution. It can be seen that in the galactic center region $\tilde{\mathcal{E}}_j(0.95)$ for the scenario with a negligible SHDM contribution has to be three times larger than the one corresponding to the case with a non negligible SHDM component. In the Andromeda region this ratio is ~ 1.8 .

For $E_{min} = 10^{20.3}$ eV $\tilde{\mathcal{E}}_j(0.95)$ increases (see the left panel of Fig. 9 of appendix C). In this case $\tilde{\mathcal{E}}_j(0.95)$ ranges from 6.3×10^6 km² yr sr to 2.5×10^7 km² yr sr. Also the relative importance of the SHDM component of the flux increases for increasing values of the minimum energy, making the differences between the two scenarios considered more important. In particular, in the galactic center region, $\tilde{\mathcal{E}}_j(0.95)$ for the case with a negligible SHDM contribution has to be 17 times larger than the one corresponding to the case with a non negligible SHDM component. Also, in the Andromeda region it has to be ~ 7.5 times larger (see the right panel of Fig. 9 of appendix C). Therefore, the observation of at least one event in one of those pixels for a given exposure can be used to discriminate between these two different scenarios.

The probability to observe at least one event in a given set of pixels is given by,

$$P_{set}(n \geq 1 | E_{min}, \mathcal{E}) = 1 - \exp \left[- \sum_{j \in S_p} \mu_j(E_{min}, \mathcal{E}) \right], \quad (2.14)$$

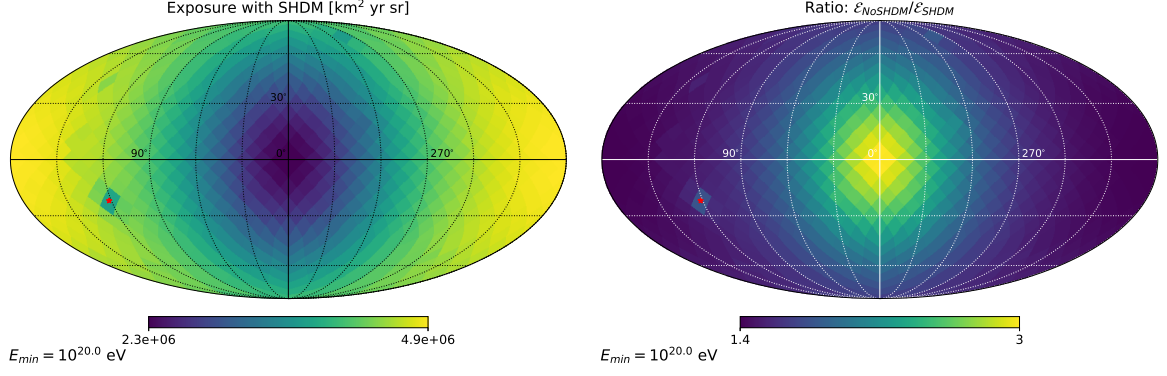


Figure 7. Left panel: Exposure required to observe at least one event in each pixel with 0.95 probability including all contributions considered. Right panel: Ratio between the exposure required to observe at least one event in each pixel with 0.95 probability without and with the inclusion of a non negligible SHDM component. The minimum energy is $E_{min} = 10^{20}$ eV and the red star corresponds to the position of Andromeda.

where S_p is the set of pixels considered. Fig. 8 shows the probability to observe at least one event in two different sets of pixels as a function of the exposure for the two scenarios considered and for $E_{min} = 10^{20}$ eV and $E_{min} = 10^{20.3}$ eV. The two sets of pixels considered are: *i*) the four pixels closer to the galactic center, S_{GC} , and *ii*) the two hottest pixels in the surroundings of Andromeda (see Fig. 6), S_{M31} . From the figure it can be seen that the probability reaches one for smaller values of the exposure in the scenarios with a non negligible SHDM contribution. Also, the probability reaches one for smaller values of the exposure in the case of S_{GC} , as expected.

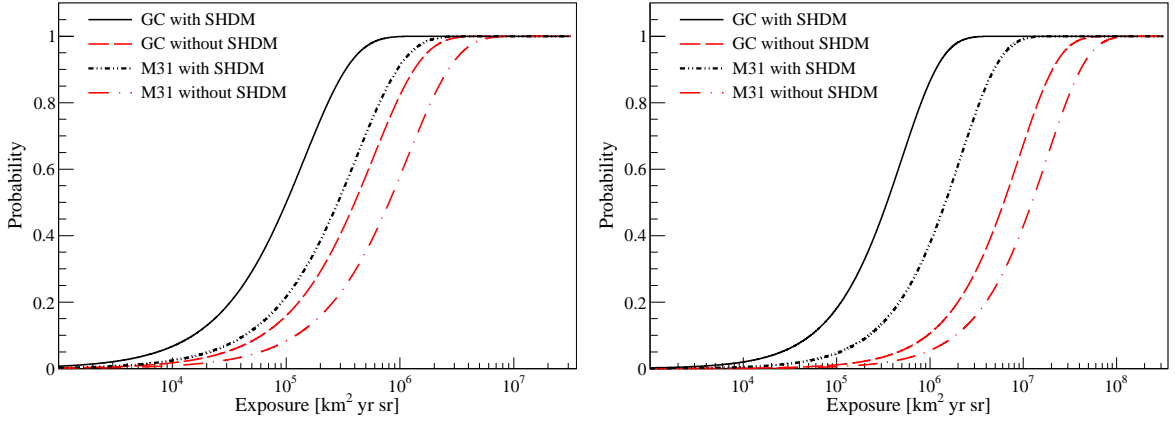


Figure 8. Probability to observe at least one event in a given set of pixels (see text for details) as a function of the exposure for $E_{min} = 10^{20}$ eV (left panel) and $E_{min} = 10^{20.3}$ eV (right panel).

For a given set of pixels let us consider the exposure for which the probability to observe at least one event in the scenario without a component originated from SHDM is 0.1, which is denoted as \mathcal{E}_{10} . Therefore, if for this value of the exposure reached by a given observatory at least one event is observed in this set of pixels, the null hypothesis that states that the UHECR flux is the one corresponding to the astrophysical origin is rejected at 90% confidence level (CL). The probability to observe at least one event for the exposure value \mathcal{E}_{10} in a given

set of pixels but for the model that includes a SHDM contribution considered before gives the probability to reject the null hypothesis. This probability will be denoted as P_{rej} . Table 1 shows the values of \mathcal{E}_{10} and P_{rej} for $E_{min} = 10^{20}$ eV and $E_{min} = 10^{20.3}$ eV and for the two sets of pixels considered. From the table it can be seen that for $E_{min} = 10^{20}$ eV, P_{rej} is smaller than 0.5 for the two sets of pixels considered (0.34 and 0.26 for S_{GC} and S_{M31} , respectively). Note that the Auger exposure at present is approximately 8×10^4 km² yr sr [40] and it can reach values of order of 2×10^5 km² yr sr at the end of its life [41]. Therefore, with Auger data it will be possible to performed the proposed test for $E_{min} = 10^{20}$ eV. For $E_{min} = 10^{20.3}$ eV P_{rej} is larger than 0.5, i.e. 0.85 and 0.59 for S_{GC} and S_{M31} , respectively. The set S_{M31} requires a larger exposure but it can be used to test independently the null hypothesis.

E_{min} [eV]	\mathcal{E}_{10} [km ² yr sr] for S_{GC}	P_{rej} for S_{GC}	\mathcal{E}_{10} [km ² yr sr] for S_{M31}	P_{rej} for S_{M31}
10^{20}	6.1×10^4	0.34	1.2×10^5	0.26
$10^{20.3}$	9.4×10^5	0.85	1.9×10^6	0.59

Table 1. \mathcal{E}_{10} and P_{rej} for the two sets of pixels considered and for $E_{min} = 10^{20}$ eV and $E_{min} = 10^{20.3}$ eV.

Although for $E_{min} = 10^{20.3}$ eV larger values of the exposure are required for the probability to saturate, it allows to reject the null hypothesis by using both set of pixels considered. The reason for this behavior has to do with the fact that in this energy range the contribution of the astrophysical component decreases much faster (the flux goes as $\sim E^{-5}$) than the one corresponding to the SHDM component (see Fig. 3) and then the component originated from SHDM decay becomes more important.

3 Conclusions

In this article the possibility to identify a scenario in which there is a non-negligible but minority component, originated from the decay of SHDM particles, that dominates the UHECR flux beyond the suppression has been studied. Due to the expected small flux of UHECRs originated from the decay of SHDM particles these studies have been done in the context of the next generation UHECR observatories which are planed to have larger exposures compared with current ones. Besides the contribution from the galactic halo, the contribution from extragalactic halos has also been considered.

The scenario in which the SHDM particles have a mass of $10^{22.3}$ eV and a decay time of $\tau_X = 5.4 \times 10^{22}$ yr has been considered. The values of these two parameters are compatible with current constraints. For this scenario it has been found that the halo of the Andromeda galaxy is the one that most contributes to the SHDM extragalactic component. For a uniform exposure of 10^6 km² yr sr the mean number of events expected from Andromeda, above 10^{20} eV, is of order one. The null hypothesis which states that the UHECR flux is composed by a uniform flux of astrophysical origin has a $\sim 85\%$ probability to be rejected considering a set of pixels in the region of the sky close to the galactic center and for primary energies above $10^{20.3}$ eV. In this case the exposure required is $\sim 9.4 \times 10^5$ km² yr sr. For larger values of the exposure, i.e. 1.9×10^6 km² yr sr, the null hypothesis has $\sim 59\%$ probability to be rejected considering the hottest pixels in the surroundings of Andromeda and considering also the same energy range. This can be used as an independent test. Therefore, the next generation

UHECR observatories that reach exposures of the order of $10^6 \text{ km}^2 \text{ yr sr}$ will be able to identify or even constraint the scenarios in which there is a minority component originated from the decay of SHDM particles.

A Cosmic rays of astrophysical origin

The fitting function of Ref. [35] is used to describe the component of astrophysical origin, which is given by,

$$J(E) = J_a \begin{cases} \left(\frac{E}{E_a}\right)^{-\gamma_1} & E \leq E_a \\ \left(\frac{E}{E_a}\right)^{-\gamma_2} \frac{1 + \left(\frac{E_a}{E_s}\right)^{\Delta\gamma}}{1 + \left(\frac{E}{E_s}\right)^{\Delta\gamma}} & E > E_a \end{cases}, \quad (\text{A.1})$$

where J_a is a normalization constant, $E_a = 5.08 \times 10^{18} \text{ eV}$, $E_s = 3.9 \times 10^{19} \text{ eV}$, $\gamma_1 = 3.293$, $\gamma_2 = 2.53$, and $\Delta\gamma = 2.5$.

The integral flux for $E > E_a$, which is used in the calculations, is given by,

$$J(> E) = J_a \left[1 + \left(\frac{E_a}{E_s}\right)^{\Delta\gamma} \right] \left(\frac{E_a}{E_s}\right)^\gamma \left(\frac{E}{E_s}\right)^{1-\gamma-\Delta\gamma} \frac{E_s}{\gamma + \Delta\gamma - 1} \times {}_2F_1\left(1, \frac{\gamma + \Delta\gamma - 1}{\Delta\gamma}, \frac{\gamma + 2\Delta\gamma - 1}{\Delta\gamma}, -\left(\frac{E_s}{E}\right)^{\Delta\gamma}\right), \quad (\text{A.2})$$

where ${}_2F_1(a, b, c, z)$ is the hypergeometric function.

B Angular distribution

The integral in Eq. (2.9) can be performed analytically for the case of the Burkert dark matter profile. It can be expressed as,

$$J(E, \theta) = \frac{\text{sr}^{-1}}{4\pi M_X c^2 \tau_X} \frac{dN}{dE} \times \begin{cases} I_1(\theta, D) + I_2(\theta, D) & 0 \leq \theta \leq \frac{\pi}{2} \\ I_2(\theta, D) - I_1(\theta, D) & \frac{\pi}{2} < \theta \leq \frac{\pi}{2} \end{cases}, \quad (\text{B.1})$$

where subscripts i and s are omitted for clarity and,

$$I_1(\theta, D) = \frac{\rho_B r_B}{2} \left[\frac{r_B}{\sqrt{D^2 \sin^2 \theta + r_B^2}} \left(\arctan \left[\frac{D |\cos \theta|}{\sqrt{D^2 \sin^2 \theta + r_B^2}} \right] + \operatorname{artanh} \left[\frac{r_B |\cos \theta|}{\sqrt{D^2 \sin^2 \theta + r_B^2}} \right] \right) - \xi_1(\theta, D) \right], \quad (\text{B.2})$$

$$I_2(\theta, D) = \frac{\rho_B r_B}{2} \left[\frac{r_B}{\sqrt{D^2 \sin^2 \theta + r_B^2}} \left(\frac{\pi}{2} + \operatorname{artanh} \left[\frac{r_B |\cos \theta|}{\sqrt{D^2 \sin^2 \theta + r_B^2}} \right] \right) - \xi_2(\theta, D) \right]. \quad (\text{B.3})$$

Here,

$$\xi_1(\theta, D) = \begin{cases} \frac{r_B}{\sqrt{D^2 \sin^2 \theta - r_B^2}} \arctan \left[\frac{|\cos \theta| \sqrt{D^2 \sin^2 \theta - r_B^2}}{D \sin^2 \theta + r_B} \right] & D \sin \theta > r_B \\ \sqrt{\frac{D - r_B}{D + r_B}} & D \sin \theta = r_B \\ \frac{r_B}{\sqrt{r_B^2 - D^2 \sin^2 \theta}} \operatorname{artanh} \left[\frac{|\cos \theta| \sqrt{r_B^2 - D^2 \sin^2 \theta}}{D \sin^2 \theta + r_B} \right] & D \sin \theta < r_B \end{cases} \quad (\text{B.4})$$

and

$$\xi_2(\theta, D) = \begin{cases} \frac{r_B}{\sqrt{D^2 \sin^2 \theta - r_B^2}} \arctan \left[\frac{\sqrt{D^2 \sin^2 \theta - r_B^2}}{r_B} \right] & D \sin \theta > r_B \\ 1 & D \sin \theta = r_B \\ \frac{r_B}{\sqrt{r_B^2 - D^2 \sin^2 \theta}} \operatorname{artanh} \left[\frac{\sqrt{r_B^2 - D^2 \sin^2 \theta}}{r_B} \right] & D \sin \theta < r_B \end{cases} \quad (\text{B.5})$$

C Required exposure for larger minimum energy

The left panel of Fig. 9 shows the exposure required to observe at least one event in each pixel for $E_{min} = 10^{20.3}$ eV and $p_0 = 0.95$ and for the case in which the contribution from SHDM is non negligible. The right panel of the figure shows the ratio between the exposure required to observed at least one event in each pixel with 0.95 probability in the scenario without a SHDM contribution and in the one with a non negligible SHDM contribution.

Acknowledgments

A. D. S. is member of the Carrera del Investigador Científico of CONICET, Argentina. This work is supported by ANPCyT PICT-2015-2752, Argentina. The authors thank the members of the Pierre Auger Collaboration for useful discussions and R. Clay for reviewing the manuscript.

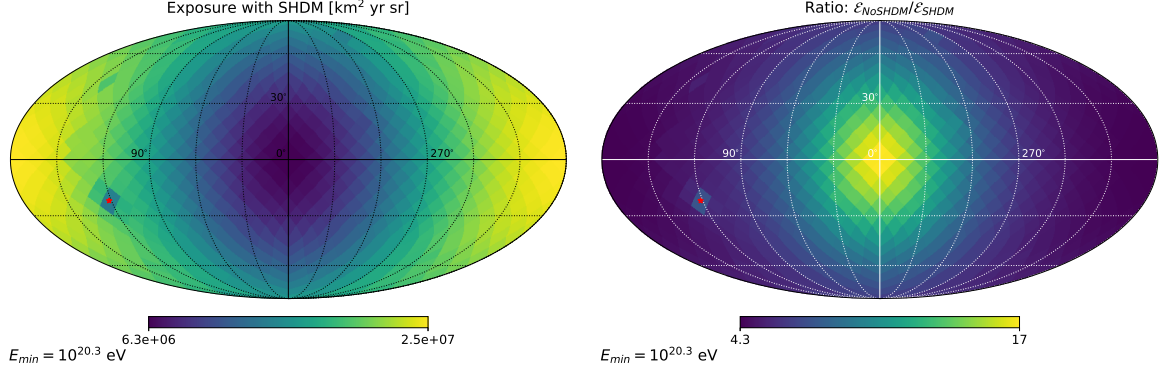


Figure 9. Left panel: Exposure required to observe at least one event in each pixel with 0.95 probability including all contributions considered. Right panel: Ratio between the exposure required to observe at least one event in each pixel with 0.95 probability without and with the inclusion of the SHDM component. The minimum energy is $E_{min} = 10^{20.3}$ eV and the red star corresponds to the position of Andromeda.

References

- [1] D. Ivanov, for the Pierre Auger Collaboration and the Telescope Array Collaboration, *Report of the Telescope Array-Pierre Auger Observatory Working Group on Energy Spectrum*, *PoS(ICRC2017)* (2017) 498.
- [2] P. Aab et al. (The Pierre Auger collaboration), *Depth of Maximum of Air-Shower Profiles at the Auger Observatory: Measurements at Energies above $10^{17.8}$ eV*, *Phys. Rev. D* **90** (2014) 122005.
- [3] R. Abbasi et al. (The Telescope Array collaboration), *Depth of Ultra High Energy Cosmic Ray Induced Air Shower Maxima Measured by the Telescope Array Black Rock and Long Ridge FADC Fluorescence Detectors and Surface Array in Hybrid Mode*, *Astrophys. J.* **858** (2015) 76.
- [4] V. de Souza for The Pierre Auger Collaboration and Telescope Array Collaboration, *Testing the agreement between the X_{max} distributions measured by the Pierre Auger and Telescope Array Observatories*, *PoS (ICRC2017)* (2017) 522.
- [5] P. Aab et al. (The Pierre Auger collaboration), *Observation of a large-scale anisotropy in the arrival directions of cosmic rays above 8×10^{18} eV*, *Science* **357** (2017) 1266.
- [6] P. Aab et al. (The Pierre Auger collaboration), *An indication of anisotropy in arrival directions of ultra-high-energy cosmic rays through comparison to the flux pattern of extragalactic gamma-ray sources*, *Astrophys. J.* **853** (2018) L29.
- [7] U. Giaccari for The Pierre Auger Collaboration, *Arrival directions of the highest-energy cosmic rays detected by the Pierre Auger Observatory*, *PoS (ICRC2017)* (2017) 483.
- [8] P. Aab et al. (The Pierre Auger collaboration), *Searches for Anisotropies in the Arrival Directions of the Highest Energy Cosmic Rays Detected by the Pierre Auger Observatory*, *Astrophys. J.* **804** (2015) 15.
- [9] R. Abbasi et al. (The Telescope Array collaboration), *Indications of intermediate -scale anisotropy of cosmic rays with energy greater than 57 EeV in the Northern sky measured with the surface detector of of the Telescope Array experiment*, *Astrophys. J.* **790** (2014) L21.
- [10] K. Kawata et al. (The Telescope Array collaboration), *Ultra-high-energy cosmic-ray hotspot observed with the Telescope Array surface detector*, *PoS (ICRC2015)* (2016) 2016.

- [11] E. Alcantara, L. Anchordoqui, and J. Soriano, *Hunting for super-heavy dark matter with the highest-energy cosmic rays*, *Phys. Rev. D* **99** (2019) 103016.
- [12] G. Medina-Tanco and A. Watson, *Dark matter halos and the anisotropy of ultra-high energy cosmic rays*, *Astropart. Phys.* **12** (1999) 25.
- [13] R. Aloisio and F. Totorici, *Super heavy dark matter and UHECR anisotropy at low energy*, *Astropart. Phys.* **29** (2008) 307.
- [14] O. Kalashev et al., *Global anisotropy of arrival directions of ultra-high-energy cosmic rays: capabilities of space-based detectors*, *JCAP* **0803** (2008) 003.
- [15] R. Aloisio, S. Matarrese, and A. Olinto, *Super Heavy Dark Matter in light of BICEP2, Planck and Ultra High Energy Cosmic Rays Observations*, *JCAP* **08** (2015) 024.
- [16] O. Kalashev and M. Kuznetsov, *Heavy decaying dark matter and large-scale anisotropy of high-energy cosmic rays*, *JETP Lett.* **106** (2017) 73.
- [17] L. Marzola and F. Urban, *Astropart. Phys.* **93** (2017) 56.
- [18] V. Kuzmin, I. Tkachev, *Ultrahigh-energy cosmic rays, superheavy long living particles, and matter creation after inflation*, *JETP Lett.* **68** (1998) 271.
- [19] D. Chung, E. Kolb, and A. Riotto, *Superheavy dark matter*, *Phys. Rev. D* **59** (1998) 023501.
- [20] V. Kuzmin and I. Tkachev, *Matter creation via vacuum fluctuations in the early universe and observed ultrahigh-energy cosmic ray events*, *Phys. Rev. D* **59** (1999) 123006.
- [21] V. Kuzmin and I. Tkachev, *Ultrahigh-energy cosmic rays and inflation relics*, *Phys. Rep.* **320** (1999) 1999.
- [22] O. Kalashev and M. Kuznetsov, *Constraining heavy decaying dark matter with the high energy gamma-ray limits*, *Phys. Rev. D* **94** (2016) 063535.
- [23] P. Sommers, *Cosmic ray anisotropy analysis with a full-sky observatory*, *Astropart. Phys.* **14** (2001) 271.
- [24] C. Barbot, *Decay of super-heavy particles: user guide of the SHdecay program*, *Comput. Phys. Commun.* **157** (2004) 63.
- [25] R. Protheroe and P. Biermann, *A new estimate of the extragalactic radio background and implications for ultra-high-energy γ -ray propagation*, *Astropart. Phys.* **6** (1996) 45, R. Protheroe and P. Biermann, *Astropart. Phys. Erratum-ibid* **7** (1997) 181.
- [26] <https://github.com/CRPropa/CRPropa3-data>.
- [27] A. Burkert, *The structure of dark matter halos in dwarf galaxies*, *Astrophys. J.* **447** (1995) L25.
- [28] F. Nesti and P. Salucci, *The Dark Matter halo of the Milky Way*, *JCAP* **1307** (2013) 016.
- [29] M. Lisanti et al., *A Search for Dark Matter Annihilation in Galaxy Groups*, *Phys. Rev. Lett.* **120** (2018) 101101.
- [30] M. Lisanti et al., *Mapping Extragalactic Dark Matter Annihilation with Galaxy Surveys: A Systematic Study of Stacked Group Searches*, *Phys. Rev. D* **97** (2018) 063005.
- [31] R. Brent Tully, *Galaxy Groups: A 2MASS Catalog*, *Astrophys. J.* **149** (2015) 171.
- [32] E. Kourkchi and R. Brent Tully, *Galaxy Groups Within 3500 km s^{-1}* , *Astrophys. J.* **853** (2017) 16.
- [33] C. Bleve for the Pierre Auger Collaboration, *Update of the neutrino and photon limits from the Pierre Auger Observatory*, *PoS (ICRC2015)* (2015) 1103.
- [34] R. Batista et al., *CRPropa 3-a Public Astrophysical Simulation Framework for Propagating Extraterrestrial Ultra-High Energy Particles*, *JCAP* **1605** (2016) 038.

- [35] F. Fenu for the Pierre Auger Collaboration, *The cosmic ray energy spectrum measured using the Pierre Auger Observatory*, *PoS (ICRC2017)* (2017) 486.
- [36] V. Berezhinsky and S. Grigor'eva, *A bump in the ultra-high energy cosmic ray spectrum*, *Astron. Astrophys.* **199** (1988) 1.
- [37] J.H. Adams Jr. et al. (The JEM-EUSO Collaboration), *The JEM-EUSO mission: An introduction*, *Experimental Astronomy* **40** (2015) 3.
- [38] L. Anchordoqui et al., *UHECRs with POEMMA*, arxiv:1907.03694.
- [39] K. Górski et al., *HEALPix: A framework for high-resolution discretization and fast analysis of data distributed on the sphere*, *Astrophys. J.*, **622** (2005) 759.
- [40] V. Verzi for the Pierre Auger Collaboration, *Measurement of the energy spectrum of ultra-high energy cosmic rays using the Pierre Auger Observatory*, *PoS (ICRC2019)* (2019) 450.
- [41] R. Batista et al., *Open Questions in Cosmic-Ray Research at Ultrahigh Energies*, *Front. Astron. Space Sci.* **6** (2019) 26.